Discretized Simulation of Vortex Sheet Evolution with Buoyancy and Surface Tension Effects

Robert G. Zalosh*
Mt. Auburn Research Associates, Inc., Newton, Mass.

The discrete vortex method previously used by Rosenhead and others to compute the roll-up of a vortex sheet in a single fluid is extended to the situation in which the vortex sheet is a horizontal interface separating a lighter inviscid fluid above from a heavier fluid below. The stabilizing effects of gravity and surface tension are included in a discretized circulation equation used to calculate the circulations of individual vortices during the course of the computation. Calculations show the evolution of the interface under stable, unstable, and marginally unstable conditions as given by linear Kelvin-Helmholtz instability theory. Under stable conditions, finite amplitude disturbances oscillate with a period slightly larger than predicted by classical theory for infinitesimal perturbations. For unstable conditions, the finite amplitude growth rate is much smaller than the corresponding linearized growth rate for infinitesimal disturbances. Under marginally unstable conditions, small irregularities along the interface cause numerical difficulties before the maximum disturbance amplitude and extent of roll-up has been computed.

I. Introduction

THE interfacial instability of a vortex sheet separating two fluids is a classical problem that has attracted theorists ever since Kelvin formulated his linear instability analysis (Chandrasekhar[1]). Recently, there has been renewed interest in the interfacial shear instability problem because of its relevance to oil slick control techniques. Oil droplet formation at the oil/water interface and the subsequent entrainment of the oil droplets into the water current are responsible for oil loss under conventional containment booms. The purpose of this paper is to describe a numerical method that willl simulate the evolution of a vortex sheet interface under unstable conditions, and also under the stabilizing effect of gravity and surface tension. The application of this method to the contained oil slick problem is presented in another paper.[2]

The discrete vortex method developed here is an extension of a technique used by earlier investigators to simulate vortex sheets. Rosenhead[3] first used the discrete vortex method to calculate the roll-up of a vortex sheeet separating two parallel streams of the same fluid. Rosenhead's discrete vortex simulation showed a vortex sheet with an initial sinusoidal perturbation rolling up smoothly into periodic spirals with local concentrations of vorticity.

Birkhoff and Fisher[4] took issue with the assertion that a vortex sheet in an inviscid fluid can roll-up smoothly with an indefinite concentration of vorticity. They demonstrated that the energy invariance of a set of point vortices prevents any two vortices from getting arbitrarily close to each other. Furthermore, the approach of one pair of vortices must be accompanied by the recession of another pair. Birkhoff and Fisher supplemented their theoretical arguments with their own version of Rosenhead's computation. They employed a slightly different initial distribution of vortices along the sinusoidal perturbation, and the time step in their Runge-Kutta integration routine was smaller than Rosenhead's time step. Their vortex sheet at late times was more contorted and irregular than Rosenhead's smooth spiral. They conclude that viscosity is essential to produce a smooth rolling-up of real vortex sheets.

Hama and Burke[5] also obtained a highly irregular vortex sheet at late times when they repeated Rosenhead's calculations. They attempted to suppress the irregularity by accounting for the nonuniform distribution of vorticity along the initial sinusoidal displacement of the sheet. By spacing their vortices unevenly initially, they calculated a smooth rolling-up process similar to Rosenhead's configuration. Hama and Burke conclude that the discrete vortex method can model the formation of local concentrations of vorticity and the overall form of the vortex sheet. Abernathy and Kronauer[6] reach a similar conclusion based on their calculations of vortex street formation using a double row of point vortices.

Fink and Soh[7] offer an interesting explanation for the late time chaotic shape of the vortex sheet obtained by Birkhoff and Fisher[4] and Hama and Burke[5] (and observed in several calculations with the discrete vortex method of the roll-up of trailing edge vortex sheets behind airfoils). Fink and Soh explain that the late time randomness is a consequence of the representation of a continuous distribution of vorticity by a set of discrete vortices. They show that the Cauchy principal value evaluation of the Biot-Savart integral for the induced velocity of a segmented continuous vortex sheet includes a logarithmic term that is not accounted for in the discrete vortex representation of the sheet. The logarithmic term accounts for the self-induced velocity of a segment of the vortex sheet, whereas a discrete line vortex has no self-induced velocity.

The intent in this paper is to formulate and apply the discrete vortex method for the case where the evolution of the vortex sheet is influenced by the stabilizing effects of buoyancy and surface tension. Thus, the vortex sheet here coincides with an interface between two fluids – for example, the oil/water interface of a contained oil slick. We accept the late time inaccuracies associated with the discretization of the vortex sheet. Instead, we demonstrate that the discrete vortex method is a useful tool for calculating early time disturbance growth rates and the overall form of the interface for disturbance amplitudes outside the realm of linear Kelvin-Helmholtz stability theory.

Presented at the 2nd Computational Fluid Dynamics Conference, Hartford, Conn., June 19-20, 1975. (No preprints, Bound Volume pp. 205-219); submitted June 20, 1975; revision received June 17, 1976. This research was supported by the U.S. Coast Guard under Contract DOT-CG-41882-A. The opinions or assertions contained herein are not to be construed as official or reflecting the views of the Commandant or the U.S. Coast Guard at large. The inst and assistance of LCDR Donald Jensen of the Coast Guard, technical monitor for this project, is gratefully acknowledged. The author is also grateful for the many helpful discussions with Drs. Sheldon L. Kahalas and Brian L. Murphy of Mt. Auburn Research Associates, Inc.

Index categories: Hydrodynamics; Subsonic and Transonic Flow.

*Presently with Factory Mutual Research Corp., Norwood, Mass. Member AIAA.

According to linear theory[1] a horizontal vortex sheet in the x-y plane separating two different inviscid incompressible fluids streaming in the x direction, will at some time t have a displacement of the form $A_0 \exp(ikx+nt)$, where A_0 and k are the amplitude and wave number of an initial disturbance (see Fig. 1). The dispersion relation for n is

$$n=\frac{ik\Delta U(\rho_2-\rho_1)}{2(\rho_1+\rho_2)}+\left(\frac{k^2(\Delta U)^2\rho_1\rho_2}{(\rho_1+\rho_2)^2}-\frac{\sigma k^3+gk(\rho_2-\rho_1)}{\rho_1+\rho_2}\right)^{1/2} \tag{1}$$

In Eq. (1), ΔU is the velocity difference across the interface, ρ_1 and ρ_2 are the densities of the upper and lower fluids, respectively, g is the acceleration of gravity, and σ is the interfacial surface tension. The relative sizes of the two terms in the brackets in Eq. (1) determine whether a given disturbance will grow or oscillate in time. The usual disturbance of interest corresponds to the wave number k_c that maximizes the growth rate. This critical wave number is

$$k_c=\sqrt{g(\rho_2-\rho_1)/\sigma} \tag{2}$$

Substitution of Eq. (2) into Eq. (1) yields the following equation for the critical velocity difference, ΔU_c, for a growing disturbance.

$$(\Delta U_c)^2=\frac{2(\rho_1+\rho_2)}{\rho_1\rho_2}\sqrt{\sigma g(\rho_2-\rho_1)} \tag{3}$$

Thus, according to linear theory, velocity differences larger than ΔU_c represent unstable configurations, and velocity differences less than ΔU_c are stable. In the following section, the discrete vortex formulation of this problem is derived. In Secs. III, IV, and V the results of calculations with the discrete vortex method for the cases of unstable, stable, and marginally unstable conditions, respectively, as predicted by Eq. (3), are presented.

II. Discrete Vortex Method

In the discrete vortex method, one wavelength of the vortex sheet is simulated by a set of N point vortices (line vortices lying in the surface of the vortex sheet). For each point vortex at location (x_j,y_j), we associated an infinite number of identical vortices with coordinates $(x_j\pm\lambda,y_j)$, $(x_j\pm2\lambda,y_j)$... where λ is the wavelength of the disturbance. The velocity components induced at the ith vortex by the jth vortex and all its counterparts at the other wavelengths are[8]

$$\bar{U}_{ij}=\frac{\Gamma_j}{2\lambda}\frac{\sinh k(y_i-y_j)}{\cosh k(y_i-y_j)-\cos k(x_i-x_j)} \tag{4a}$$

$$\bar{V}_{ij}=-\frac{\Gamma_j}{2\lambda}\frac{\sin k(x_i-x_j)}{\cosh k(y_i-y_j)-\cos k(x_i-x_j)} \tag{4b}$$

where $k=2\pi/\lambda$ is the wave number of the disturbance and Γ_j is the clockwise circulation of the jth vortex. The velocity components of the ith vortex induced by all of the other $N-1$ vortices in the wavelength are

$$V_{ix}=\frac{dx_i}{dt}=\sum_{i\neq j}\bar{U}_{ij} \tag{5a}$$

$$V_{iy}=\frac{dy_i}{dt}=\sum_{i\neq j}\bar{V}_{ij} \tag{5b}$$

Equations (4) and (5) have been written in a coordinate system moving with the average velocity of the upper and lower fluids. In this system the velocity components far below and above the vortex sheet are

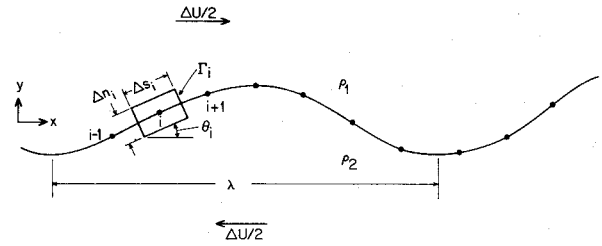

Fig. 1 Arrangement of vortices along the wavelength.

$$\lim_{y\to\pm\infty}\bar{U}=\pm\frac{1}{2\lambda}\sum_j\Gamma_j, \qquad \lim_{y\to\pm\infty}\bar{V}=0 \tag{5c}$$

The spirit of the discrete vortex method is to follow the motion of all the N vortices by integrating Eq. (5). This requires a knowledge of the circulations Γ_j as a function of time. When the interface separates two different fluids, the circulations will change because of inertial, buoyancy, and surface tension effects. We can obtain an equation for the rate of change of circulation as follows.

The fluids on both sides of the interface are assumed to be inviscid, incompressible, and have uniform, but different densities. The circulation of the ith elemental vortex is computed around a circuit that straddles the interface from midway between the i and $i-1$ vortices to midway between the i and $i+1$ vortices as shown in Fig. 1. The contributions to the circulation along the two sides of the circuit normal to the interface, Δn_i, vanish as Δn_i shrinks toward zero. If V_{1s} and V_{2s} denote the tangential velocity components of the upper and lower fluids, respectively, the clockwise circulation, Γ_i, of the ith vortex is

$$\Gamma_i=\int_{s_{i-1/2}}^{s_{i+1/2}}(V_{1s}-V_{2s})\,ds \tag{6}$$

and the rate of change of circulation is

$$\frac{d\Gamma_i}{dt}=\int_{s_{i-1/2}}^{s_{i+1/2}}\left(\frac{dV_{1s}}{dt}-\frac{dV_{2s}}{dt}\right)ds$$

$$=\Delta s_i\left(\frac{dV_{1s}}{dt}-\frac{dV_{2s}}{dt}\right)\Big|_{s_i}+0(\Delta s_i^3) \tag{7}$$

where, Δs_i is the length of the circuit parallel to the interface, i.e., $\Delta s_i=|s_{i+1}-s_{i-1}|$. The time derivatives in Eq. (7) are Lagrangian derivatives, i.e., they are evaluated moving with the ith vortex.

The acceleration terms in Eq. (7) can be evaluated from the momentum equation for each fluid. For the upper fluid

$$\frac{dV_{1s}}{dt}=-\frac{1}{\rho_1}\frac{\partial p_1}{\partial s}-g\sin\theta \tag{8}$$

where p_1 is the local pressure and θ is the local inclination of the interface with the horizontal. A similar equation with subscript 2 applies to the lower fluid. Substitution of these equations into Eq. (7) yields.

$$\frac{d\Gamma_i}{dt}=\Delta s_i\left(\frac{1}{\rho_2}\frac{\partial p_2}{\partial s}-\frac{1}{\rho_1}\frac{\partial p_1}{\partial s}\right)+0(\Delta s_i^3) \tag{9}$$

Before Eq. (9) can be used, the two pressure gradients on the right-hand side must be evaluated. Under the influence of surface tension σ there is a jump in pressure across the interface. The magnitude of the pressure jump is

$$p_2-p_1=-\sigma/R_i \tag{10}$$

where R_i^{-1}, the local curvature of the interface at the ith vortex, is

$$R_i^{-1} = \frac{\partial^2 y/\partial x^2}{[1+(\partial y/\partial x)^2]^{3/2}}\bigg|_{x_i} \tag{11}$$

Differentiation of Eq. (10) provides one equation for the two pressure gradients. The other equation is obtained as follows: The velocity of the ith vortex is defined to be the average of the two local fluid velocities at the interface. Thus the tangential acceleration of ith vortex is

$$\frac{dV_{is}}{dt} = \frac{1}{2}\left(\frac{dV_{1s}}{dt} + \frac{dV_{2s}}{dt}\right) \tag{12}$$

When the two momentum equations (8) are substituted into Eq. (12), the following equation results.

$$\frac{1}{\rho_2}\frac{\partial p_2}{\partial s} + \frac{1}{\rho_1}\frac{\partial p_1}{\partial s} = -2\frac{dV_{is}}{dt} - 2g\sin\theta \tag{13}$$

By solving Eq. (13) and the differentiated form of Eq. (10) for the two pressure gradients, and placing them in Eq. (9), the rate of change of circulation is found to be

$$\frac{d\Gamma_i}{dt} = \frac{2(\rho_2-\rho_1)}{\rho_1+\rho_2}\Delta s_i\left(g\sin\theta_i + \frac{dV_{is}}{dt}\right) - \frac{2\sigma}{\rho_1+\rho_2}\Delta s_i\frac{\partial R_i^{-1}}{\partial s} \tag{14}$$

valid to second order in Δs_i.

Equations (5) and (14) and their auxiliary relations (4) and (11) represent the basis of the discrete vortex method. They are integrated numerically to compute the positions and circulations of the elemental vortices as a function of time. For the problem under investigation, the following nondimensional variables are introduced.

$$\gamma_i = \Gamma_i/\Delta U\lambda, \quad \tau = t\Delta U/\lambda, \quad \xi_i = x_1/\lambda,$$
$$\eta_i = y_i/\lambda, \quad u_i = V_{ix}/\Delta U, \quad v_i = V_{iy}/\Delta U,$$
$$\kappa_i = \lambda R_i^{-1} \tag{15}$$

where ΔU is the nominal velocity discontinuity across the interface. In terms of these variables, the governing Eqs. (5) and (14) become

$$u_i = \frac{d\xi_i}{d\tau} = \frac{1}{2}\sum_{j\neq i}\frac{\gamma_j \sinh 2\pi(\eta_i-\eta_j)}{\cosh 2\pi(\eta_i-\eta_j) - \cos 2\pi(\xi_i-\xi_j)} \tag{16a}$$

$$v_i = \frac{d\eta_i}{d\tau} = -\frac{1}{2}\sum_{j\neq i}\frac{\gamma_j \sin 2\pi(\xi_i-\xi_j)}{\cosh 2\pi(\eta_i-\eta_j) - \cos 2\pi(\xi_i-\xi_j)} \tag{16b}$$

$$\frac{d\gamma_i}{d\tau} = (\eta_{i+1}-\eta_{i-1})Fr^{-2} + \left(\frac{1-S}{1+S}\right)\frac{dv_i}{d\tau}(\eta_{i+1}-\eta_{i-1}) + \frac{(1-S)}{(1+S)}\frac{du_i}{d\tau}(\xi_{i+1}-\xi_{i-1}) - We^{-1}(\kappa_{i+1}-\kappa_{i-1}) \tag{16c}$$

The three parameters, Fr^{-2}, We^{-1}, and S in Eq. (16c) represent the inverse Froude number, the inverse Weber number, and the density ratio. They are defined in this problem as

$$Fr^{-2} = \frac{g\lambda(\rho_2-\rho_1)}{(\Delta U)^2(\rho_1+\rho_2)}$$

$$We^{-1} = \frac{\sigma}{(\rho_1+\rho_2)\lambda(\Delta U)^2}$$

$$S = \rho_1/\rho_2$$

The initial conditions needed to implement Eq. (16) are the initial positions and circulations of the vortices. The initial coordinates (ξ_i, η_i) corresponding to a sinusoidal disturbance at the interface are

$$\xi_i = i/N, \qquad \eta_i = A_0 \sin 2\pi\xi_i \tag{17}$$

where N is the number of vortices along a wavelength and A_0 is the amplitude of the disturbance.

Small disturbance potential theory can be used to solve for the local velocity discontinuity across the vortex sheet corresponding to Eq. (17). The result[5] in terms of the nondimensional circulation γ_i is

$$\gamma_i = (1 - 2\pi A_0 \cos 2\pi\xi_i)/N \tag{18}$$

Some remarks on the computational techniques used to integrate Eqs. (16) with initial conditions (17, 18) are in order here. Equations (16) has been treated as a set of $3N$ coupled first-order equations for the $3N$ dependent variables ξ_i, η_i, γ_i, $1 \leq i \leq N$. The results presented in the following section were obtained with $N = 20$ in some cases and $N = 40$ in others.

A fourth-order Runge-Kutta numerical integration scheme was employed with a time step $\Delta\tau$ equal to 0.025 for most cases. Decreasing this time step to 0.010 resulted in less than a 1% change in the amplitude of the disturbance throughout the time interval of the computations ($\tau \leq 1.0$). The acceleration terms in Eq. (16c) were evaluated as backward time differences and the curvatures in Eq. (11) were evaluated by first-order spatial differences after determining that a second-order difference algorithm for the curvature did not produce any noticeable improvement in accuracy.

One measure of the numerical error in the computations is the change in time of net circulation per unit wavelength. It is evident from Eq. (9) that the change in net circulation over a wavelength should be zero. This is also a necessary condition to maintain the correct induced velocities at infinity as seen from Eq. (5c). At each step in the computer calculations, the circulations of all the vortices in the wavelength are summed and printed out. When the sum of the nondimensional circulations γ_i differs from unity by more than 5%, the calculations are terminated because of an unacceptable accumulation of round-off and/or truncation error. The time at which this occurred for most of the calculations with nonzero values of Fr^{-2} and We^{-1} was about $\tau = 1.0$. Presumably, this is the time at which the chaotic motion of the individual vortices, as discussed in the Introduction, causes the calculations to break down in the sense that they no longer simulate a continuous vortex sheet. Usually, the sum of the circulation was within 1% of unity for all but the last few time steps.

In most of our calculations the wavelength λ of the disturbance corresponded to the critical wave number k_c given by linear theory. This requires that the relationship between inverse Froude and Weber numbers is

$$We^{-1} = Fr^{-2}/4\pi^2 \tag{19}$$

We also made some calculations with other wavelengths and observed that the disturbance growth rate was less than the growth rate for condition Eq. (19).

In the following sections, we compare our calculations of the evolution of the interface with predictions of linear stability theory. In terms of our non-dimensional parameters, the critical inverse Froude number, Fr_c^{-2}, given by Eqs. (3 and 19) for the onset of the instability is

$$Fr_c^{-2} = \pi S/(1+S)^2 \tag{20}$$

Thus, linear stability theory predicts that infinitesimal disturbances will grow exponentially in time for $Fr^{-2} < Fr_c^{-2}$, and will oscillate for $Fr^{-2} > Fr_c^{-2}$. Our calculations demonstrate how finite amplitude disturbances behave for various values of Fr^{-2}.

III. Vortex Sheet Instability in a Uniform Fluid

For the situation in which a vortex sheet is embedded in a single uniform fluid ($S=1$ and $Fr^{-2}=We^{-1}=0$ in our notation), $d\gamma_i/d\tau=0$. This is the same case that Rosenhead,[3] Birkhoff and Fisher,[4] Hama and Burke,[5] and Fink and Soh[7] previously investigated with the discrete vortex method. The only difference between their calculations and ours for this case (besides the numerical integration routine and the time step), is that now the circulations vary along the wavelength according to Eq. (18) instead of being uniform.

The evolution of an initial disturbance with amplitude A_0 equal to 0.10 is shown in Fig. 2. It is clear from Fig. 2 that the proper initial circulation distribution Eq. (18) produces a well-behaved smooth roll-up and concentration of vorticity at the midpoint of the wavelength. The profile of the interface at $\tau=0.8$ closely resembles the profile obtained by Hama and Burke at an equivalent time. They simulated the proper initial circulation distribution by arranging their vortices at $\tau=0$ with an unequal spacing along the wavelength.

The rolled-up vortex sheet corresponding to $\tau=0.8$ in Fig. 2 has the same qualitative features exhibited by finite shear layers at moderate-to-large Reynolds numbers. Brown and Roshko[9] have published some excellent shadowgraphs illustrating the structure of the turbulent mixing layer between two different gas streams. The shadowgraphs clearly show the regular rolled-up structure of Fig. 2 for intermediate times before small-scale turbulence dominates the flow. More recently, Patnaik et al. have presented the results[10] of finite difference calculations of stably stratified horizontal shear layers. Their calculated isopycnic contours for Reynolds numbers (based on layer thickness) of the order of 100 show a rolled-up structure similar to, but not quite as convoluted as, the last vortex sheet in Fig. 2.

It would be misleading to continue the calculations much further than the time corresponding to the last profile in Fig. 2. At this time, the vortices have migrated close enough together that numerical difficulties associated with the singularity in Eqs. (16a and 16b) begin to occur, unless the time step is reduced drastically. Although the vortex sheet roll-up process is well underway at the time corresponding to the last profile in Fig. 2, the question remains as to how long it will continue to roll up. Brown and Roshko's experiments[9] with vorticity layers of finite thickness show that, at large downstream distances (presumably equivalent to late times in the present transient analysis), there is an amalgamation of adjacent vortices. In both the roll-up and amalgamation stages, fluid is entrained into and across the region of concentrated vorticity.

In Fig. 3, the early time growth rate of the disturbance is plotted for comparison with linear stability theory. The ordinate in Fig. 3 is the natural logarithm of the ratio of the amplitude of the disturbance (maximum of the absolute value of η) at time τ to the initial amplitude A_0. Linearized theory predicts an exponential growth rate, which in this plot appears as a straight line of slope π. Our calculations with $N=40$ and $A_0=0.01$ resulted in a growth rate that corresponded to a slope of 3.0, about 4% less than the linearized theory growth rate. This slightly lower growth rate is analogous to Daly's Marker and Cell Code calculations[11] for a Rayleigh-Taylor instability. Daly also found that his growth were lower than those predicted by linear theory.

The growth rate for the initial disturbance $A_0=0.10$, as shown in Fig. 3, is lower than the $A_0=0.01$ growth rate. The amplitude history for the $A_0=0.10$ case has been plotted in a linear scale as the top curve in Eig. 4. It is evident from the $Fr^{-2}=0$ curve in Fig. 4 that the growth rate is linear instead of exponential for times less than $\tau=0.4$. The time ($\tau=0.4$) at which the amplitude starts deviating from a linear growth rate corresponds to the time at which the interface begins to roll over and become double values in x (Fig. 2).

Some confirmation of the linear growth rate obtained here at early times for finite amplitude disturbances can be found in the experimental results of Brown and Roshko.[9] The latter observed that the mixing layers spread linearly with distance from some virtual origin x_0. The rate of spread for the case $S=1$ observed by Brown and Roshko was

$$\frac{A}{x-x_0}=0.38\frac{\Delta U}{U_1+U_2} \tag{21}$$

Where U_1 and U_2 denote the upper and lower stream velocities. If we make the transition from spatial instability to temporal instability by assuming that disturbances are convected downstream at the average velocity, $\frac{1}{2}(U_1+U_2)$, then

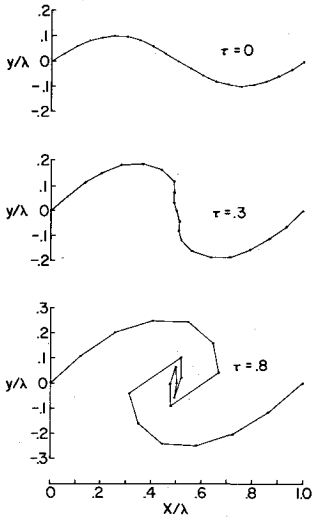

Fig. 2 Evolution of interface for $Fr^{-2}=0$, $S=1$, $N=20$, $A_0=0.10$, and $\Delta\tau=0.025$.

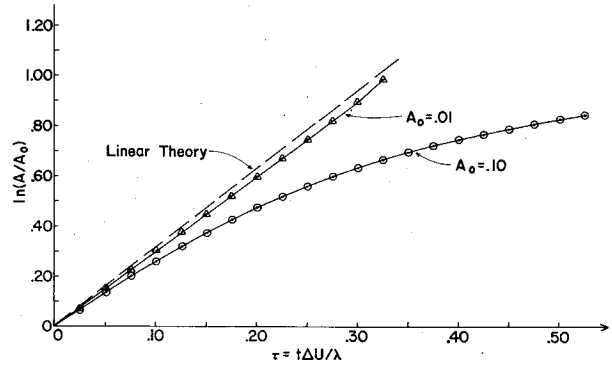

Fig. 3 Amplitude growth rate for $Fr^{-2}=0$, $S=1$, $N=40$, and $\Delta\tau=0.025$.

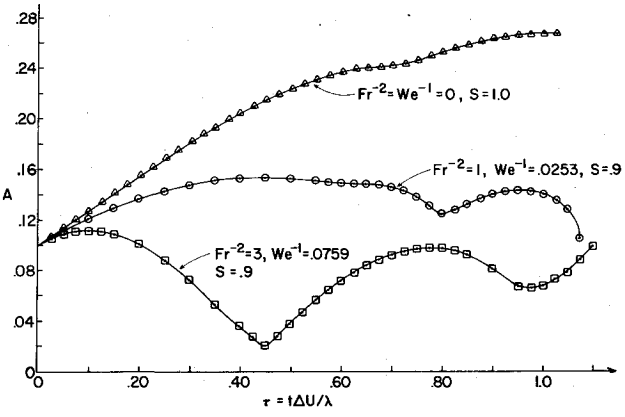

Fig. 4 Amplitude growth rate for unstable (top curve), marginally stable (middle curve), and stable (lower curve) configurations.

the Brown and Roshko result (Eq. (21)) becomes

$$A = 0.19\ \Delta U t \tag{22}$$

By measuring the slope of the top curve in Fig. 4, the amplitude growth rate calculated here is seen to be

$$A = 0.25\ \Delta U t \tag{23}$$

IV. Stabilizing Effects of Surface Tension and Buoyancy

Under the influence of surface tension and buoyancy, the evolution of the interface is dramatically different from the single fluid vortex sheet situation. The effect of finite Weber and Froude numbers on the development of the disturbance amplitude with time is shown in Fig. 4. The lower two curves in Fig. 4 represent $Fr^{-2} = 1$ and 3, and Weber numbers corresponding to the most unstable wavelength as predicted by linear theory, i.e., Eq. (19). The amplitude grows slightly at first and then oscillates in time for $Fr^{-2} = 1$ and 3. Both the period of oscillation and the maximum amplitude seem to decrease as the inverse Froude number Fr^{-2} increases.

The trends in Fig. 4 are in qualitative agreement with linear stability theory. According to linear stability theory, the critical Froude number separating monotonic growth from oscillatory behavior is given by Eq. (20). For a density ratio, S, of 0.9, Fr_c^{-2} is 0.783. Thus, the top two curves in Fig. 4 fall on either side of the critical Froude number case.

The profile of the interface at various times for $Fr^{-2} = 3$, $S = 0.9$ is shown in Fig. 5. The interface retains its sinusoidal shape, and there is no evidence of the roll-up shown in Fig. 2 for $Fr^{-2} = 0$. The points on the profiles in both Figs. 2 and 5 have been connected by straight lines and there are some small scale bumps on the profiles. Possibly, a more sophisticated numerical method for connecting the vortices and calculating curvatures, such as the techniques used by Daly,[12] would eliminate these bumps.

Some insight into the smoothing effect of surface tension on the interface can be ascertained from Fig. 6. In Fig. 6, two interfaces are shown at time $\tau = 0.50$, for $Fr^{-2} = 1$ and $S = 0.9$. The interface depicted as the top curve in Fig. 6, has evolved under the constraints of surface tension ($We^{-1} = 0.025$), whereas, the bottom interface is free of surface tension effects ($We^{-1} = 0$). The damping effect of surface tension on the small scale disturbances is readily apparent. Daly[13] has obtained analogous results in his numerical computations of the effect of surface tension on the Rayleigh-Taylor instability.

It is interesting to compare the computed periods of oscillation for stable conditions with the periods predicted by linear theory for infinitesimal perturbations. For the combination of parameters corresponding to the lower curve in Fig. 4, linear theory, i.e. Eq. (1), predicts a nondimensional period, T, equal to 1.20. The time between peaks in the lower curve in Fig. 4, $\Delta\tau = 0.70$, corresponds to one-half a period. Thus the computed period, $T = 1.40$, is larger than the linear stability theory period, $T = 1.20$. The discrepancy is not surprising since the computed period is for an initial amplitude A_0 of 0.10, which should place it outside the realm of linear theory.

The computed amplitude variation with time for a stable configuration consisting of the parameters $Fr^{-2} = 10$, $We^{-1} = 0.253$, $S = 0.90$ and for an initial amplitude $A_0 = 0.01$, within the realm of linear theory is shown in Fig. 7. The computed period of oscillation for this case, $T = 0.625$, is within 7% of the period predicted by linear theory, $T = 0.585$.

V. Marginally Unstable Case – Instability Criteria

For infinitesimal disturbances, linear Kelvin-Helmholtz stability theory predicts a clear demarcation (Eqs. (3 and 20)) between stable and unstable conditions. When the disturbances have grown to finite proportions, the situation is more complicated, and the distinction between a stable and an unstable interface can become nebulous. The classical concept that disturbance amplitude is the measure of stability can be misleading, since the amplitude is bounded, even in unstable situations. For example, the middle curve in Fig. 4 ($Fr^{-2} = 1$), which represents slightly unstable conditions, indicates that the amplitude reaches a maximum value and then begins to oscillate. Patnaik et al. observed similar results for finite amplitude Kelvin-Helmholtz waves in which viscosity replaced surface tension as a stabilizing factor.

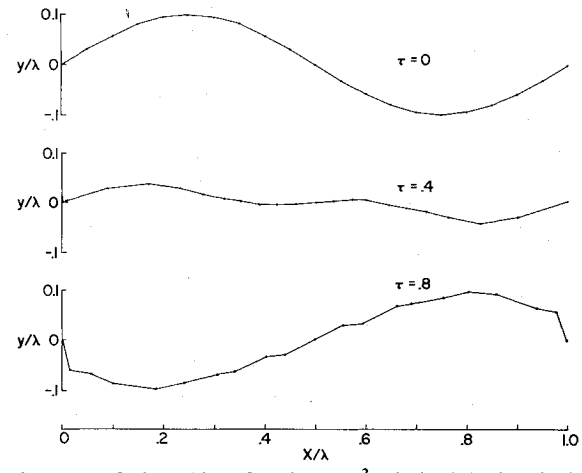

Fig. 5 Evolution of interface for $Fr^{-2} = 3$, $S = 0.9$, $A_0 = 0.10$.

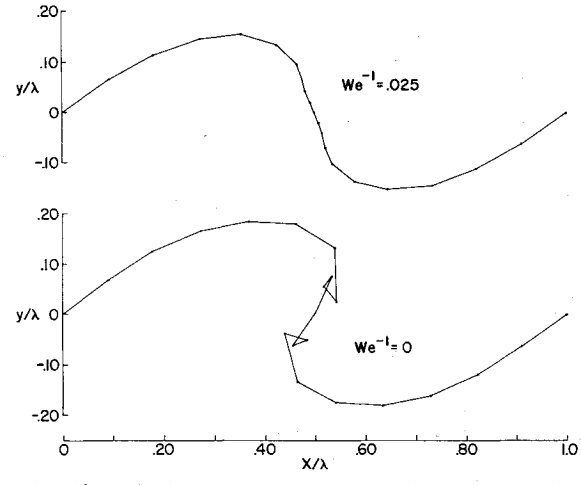

Fig. 6 Effect of Weber number on shape of interface. Both interfaces are shown at $\tau = 0.5$ for $Fr^{-2} = 1$, $S = 0.9$, $A_0 = 0.10$.

Drazin[14] examined finite amplitude effects with buoyancy and surface tnesion by perturbing the linear solution about the critical velocity (Eq. (3)). For the situation in which $\rho_1 \to \rho_2$, Drazin derived a solution for the amplitude which indicated that the disturbance should become periodic in time even for velocities slightly larger than the critical velocity given in Eq. (3). Drazin finds that an infinitesimal perturbation will eventually oscillate with a maximum amplitude, $A_{\max}$, which in our nondimensionalization scheme is given by

$$(A_{\max}/\lambda)^2 = 16(Fr\pi^{1/2} - 2)/10\pi^2 \tag{24}$$

The wave number and Weber number corresponding to Drazin's solution are given by Eqs. (2 and 19).

When the initial perturbation is small but finite, Drazin's solution indicates that the disturbance should eventually oscillate at a maximum amplitude somewhat less than Eq. (24). The period of oscillation should be long, approaching infinity for the critical Froude number, $Fr_c^2 = 4/\pi = 1.273$.

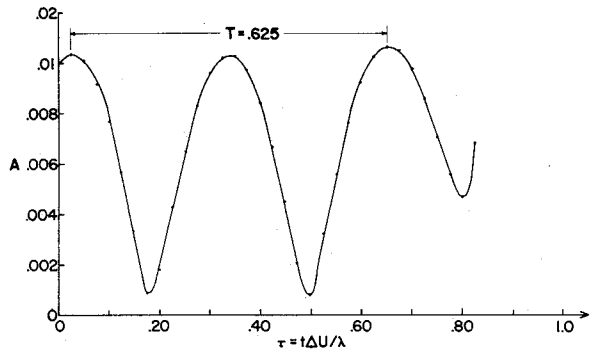

Fig. 7 Amplitude variation with time for $Fr^{-2}=0.10$, $We^{-1}=0.253$, $S=0.90$, $A_0=0.01$.

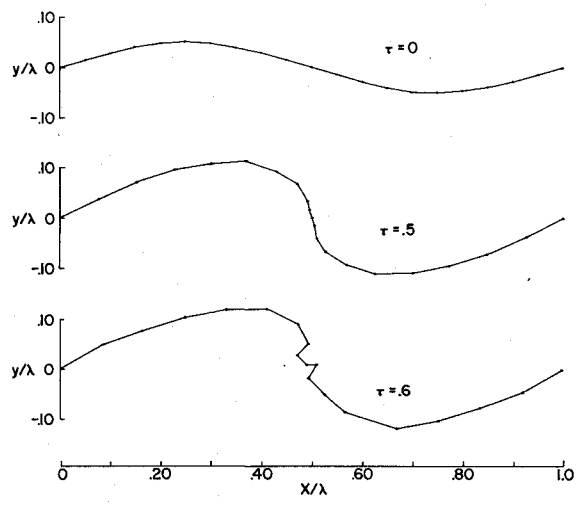

Fig. 8 Evolution of interface for $Fr^{-2}=0.7$, $S=0.99$, $A_0=0.05$.

We have attempted to confirm Drazin's predictions by computing the evolution of a marginally unstable configuration with $S=0.99$ and $Fr^2=1.438$. According to Drazin's analysis, A_{max}/λ should be somewhat less than 0.138 for these conditions. The computed evolution of the interface, starting with an initial amplitude A_0 equal to 0.05 is shown in Fig. 8. As the disturbance amplitude increases, the interface steepens and vorticity becomes concentrated, but at a much slower rate than in the case without buoyancy and surface tension (Fig. 2). The last interface, which corresponds to a time $\tau=0.6$, has a maximum nondimensional amplitude equal to 0.12, which, so far, is in accord with Drazin's analysis. Unfortunately, the interface at this time has small bumps that lead to erroneously large curvatures in the surface tension term of the circulation equation. The interface at later times (not shown in Fig. 8) becomes even more contorted and the numerical error bound on the net change in circulation over a wavelength is exceeded.

It is clear that the difficulties encountered by previous practitioners of the discrete vortex method have set in at $\tau=0.6$ in this particular calculation, and confirmation of Drazin's predicted maximum amplitude is impossible. Several different ad hoc techniques[2,7,15] have been suggested to suppress the irregularities associated with the discrete vortex method. However, most of these suppression measures apparently introduce some diffusion of vorticity, either along or away from the vortex sheet. Perhaps a more promising technique for dealing with small-scale irregularities in future work is to adopt the continuous vortex sheet formulation of Zaroodny and Greenberg.[16]

For oil/water interfaces, where instability is interpreted as fluid entrainment across the interface, this author has resorted to a semi-empirical technique for describing the late-time evolution of the interface. This approach, which is described in Ref. 2, is based on the experimental observation that interfacial steepening and roll-up is a prelude to drop formation. Thus, an empirical criterion has been established for detecting the onset of drop formation, and for smoothing the interface to simulate the detachment of the drop. A more general droplet formation/detachment analysis is still lacking and would require an improved understanding of three-dimensional interfacial instability.

VI. Conclusions

The preceding calculations have demonstrated how the discrete vortex method previously employed by Rosenhead and others to compute vortex sheet roll-up can be extended to study the behavior of an interfacial vortex sheet in the presence of surface tension and gravity effects. Based on computations with the discrete vortex model for different configurations, the following conclusions can be drawn.

1) For unstable conditions as predicted by classical Kelvin-Helmholtz instability theory, finite amplitude disturbances grow at a much smaller rate than infinitesimal disturbances. In fact, the initial growth rate is linear instead of exponential. The linear growth rate computed here is consistent with the experimental observations[9] of an initially linear rate of spread in turbulent mixing layers.

2) Shear instability manifests itself in the form of vortex sheet roll-up with accompanying entrainment of fluid into and across the region of concentrated vorticity.

3) For stable combinations of Weber number, Froude number, and density ratio, finite amplitude disturbances oscillate with a slightly longer period than predicted by classical instability theory. In two different sample cases, computed periods were about 14% and 7% larger than given by linear theory.

4) In accord with linear theory for infinitesimal perturbations, the period of oscillation of finite amplitude disturbances increases as neutral stability conditions are approached.

5) For marginally unstable conditions as given by linear theory, the disturbance amplitude first increases, but then appears to reach a maximum value. However, small-scale irregularities develop on the interface and prevent the calculations from being carried out long enough to accurately compute the value of the maximum amplitude and whether or not the interface will roll-up.

References

[1] Chandrasekhar, S., *Hydrodynamic and Hydromagnetic Stability*, Oxford University Press, 1961. §101

[2] Zalosh, R. G. and Jensen, D. S., "A Numerical Model of Droplet Entrainment from a Contained Oil Slick," *Fluid Mechanics in the Petroleum Industry*, ASME, 1975, pp. 17-27.

[3] Rosenhead, L., "The Formation of Vortices from a Surface of Discontinuity," *Proceedings of the Royal Society*, A Vol. 134, 1931, pp. 170-192.

[4] Birkhoff, G. and Fisher, J., "Do Vortex Sheets Roll Up?," Rendi Circ. Mat. Palmero, Ser. 2, Vol. 8, 1959, pp. 77-90.

[5] Hama, F. R. and Burke, E. R., "On the Rolling-up of a Vortex Sheet," University of Maryland Tech. Note, BN-220, 1960.

[6] Abernathy, F. H. and Kronauer, R. E., "The Formation of Vortex Streets," *Journal of Fluid Mechanics*, Vol. 13, 1962, pp. 1-20.

[7] Fink, P. E., and Soh, W. K., "Calculation of Vortex Sheets in Unsteady Flow and Applications in Ship Hydrodynamics," *Proceedings of the Tenth Naval Hydrodynamics Symposium*, Cambridge, Mass., June 1974.

[8] Lamb, H., *Hydrodynamics*, 6th ed., Cambridge Univ. Press, 1932. §156

[9] Brown, G. L. and Roshko, A., "On Density Effects and Large Structure in Turbulent Mixing Layers," *Journal of Fluid Mechanics*, Vol. 64, 1974, pp. 775-816.

[10] Patnaik, P. C., Sherman, F. S., and Corcos, G. M., "A Numerical Simulation of Kelvin-Helmholtz Waves of Finite Amplitude," *Journal of Fluid Mechanics*, Vol. 73, 1976, pp. 215-240.

[11] Daly, B. J., "Numerical Study of Two-Fluid Rayleigh-Taylor Instability," *Physics of Fluids*, Vol. 10, 1967, pp. 297-307.
[12] Daly, B. J., "A Technique for Including Surface Tension Effects in Hydrodynamic Calculations," *Journal of Computational Physics*, Vol. 4, 1969b, pp. 97-117.
[13] Daly, B. J., "Numerical Study of the Effect of Surface Tension on Interface Instability," *Physics of Fluid*, Vol. 12, 1969a, pp. 1340-1354.
[14] Drazin, P. G., "Kelvin-Helmholtz Instability of Finite Amplitude," *Journal of Fluid Mechanics*, Vol. 42, 1970, pp. 321-335.
[15] Moore, D. W., "A Numerical Study of the Roll-up of a Finite Vortex Sheet," *Journal of Fluid Mechanics*, Vol. 63, 1974, pp. 225-235.
[16] Zaroodny, S. J. and Greenberg, M. D., "On a Vortex Sheet Approach to the Numerical Calculation of Water Waves," *Journal of Computational Physics*, Vol. 11, 1973, pp. 440-446.